Journal of Engineering Science and Technology
Vol. 16, No. 5 (2021) 4079 - 4099


# QUANTITATIVE HAEMODYNAMIC STUDY IN RENAL ARTERY BIFURCATION USING CFD

PRANAV HEGDE[1], SHREYAS KANJALKAR[1], S. M. ABDUL KHADER[1], B. GOWRAVA SHENOY[1,*], B. RAGHUVIR PAI [1], MASAAKI TAMAGAWA[2], RAVINDRA PRABHU[3], D. SRIKANTH RAO[1]

[1]Department of Mechanical and Manufacturing Engineering, Manipal Institute of Technology, Manipal Academy of Higher Education, Manipal, Karnataka, India
[2]Department of Biological Functions Engineering, Graduate School of Life Sciences and System Engineering, Kyushu Institute of Technology, Japan
[3]Department of Nephrology, Kasturba Medical College, Manipal Academy of Higher Education, Manipal, Karnataka, India
*Corresponding Author: gowrav.shenoy@manipal.edu

## Abstract

Computational Fluid Dynamics facilitates in the quantitative analysis of haemodynamic processes of *in vivo* cardiovascular systems. The objective of the present study is to examine the effects of different branching angles of diseased renal arteries with respect to the abdominal aorta on its flow characteristics. Secondly, simulation of normal renal arteries at similar branching angles were also done as a baseline for comparison to comprehend if geometry played a role in the endothelial proliferation in renal artery stenosis. Idealistic renal artery models generated from the digital image of computerized tomography scan were used, with bifurcation angles at the junction ranging from 30° to 90° at successive intervals of 15°. Virtual stenosis of a degree below and above 80% by diameter were generated on the right and left renal artery respectively. The models were discretized using a hybrid polyhedral mesh. Parameters such as time-averaged velocity, time-averaged wall shear stress, pressure difference and fractional flow reserve were used to analyse the flow characteristics. Stenosed renal arteries with higher angulation was found to have larger flow recirculation zones, higher pressure gradient near the Ostia and was observed to experience greater amounts of shear stress at the region of stenosis. For the same degree of stenosis (above 80%), the blockage tended to increase from 18% to 25%, as the angle increased. The effect of angulation was observed to alter the flow characteristics significantly in the stenosed arteries. Critically stenosed (above 80%) renal arteries at a bifurcation angle above 45° showed signs of ischemia.

Keywords: Fractional flow reserve, Haemodynamic, Renal artery bifurcation, Recirculation zone, Time average wall shear stress.

## 1. Introduction

Atherosclerosis, the process of narrowing of the arterial walls due to the build-up of fats, cholesterol and lipoproteins, is one of the main causes of renal artery stenosis (RAS) [1]. It leads to renovascular hypertension in one out of every twenty patients diagnosed with this disease [2, 3]. The reduction in the amount of blood flow results in the activation of the renin-angiotensin-aldosterone system (RAAS) by the kidney; increasing the blood pressure [4]. Clinical trials conducted in order to identify the predictors of RAS in patients diagnosed with coronary artery disease were renal insufficiency and hypertension in separate cases or in conjunction with other chronic diseases like diabetes mellitus [5]. Experimental studies done using the data obtained from various patients have proved that geometry of the artery is also one of the factors which can influence plaque formation [6].

Geometric features like regions where flow separation of blood occurs, primarily in the artery junctions are considered to be more prone to plaque formation [7]. In these regions of bifurcations, the occurrence of recirculation of blood due to unusual flow patterns tends to deposit lipids and other materials leading to vasoconstriction. Moreover, factors involved with the geometry of the junctions like branching ratio and branching angle have known to cause variations in blood flow and shear stresses along the arterial wall, justifying the fact that it is one of the geometric risk factors for early development of atherosclerosis [8]. The human vasculature is known to vary from person to person which contribute to the variances in cardiovascular diseases among the general population; given that haemodynamic variables of the flow, mediated by the arterial lumen influence the rate and location of atherogenesis [9, 10]. Therefore, extensive research work on the factors influencing RAS have been carried out to find preventive methods, to conduct better diagnosis and to find a cure.

Assessment of RAS to analyse its functional aspects are currently accomplished using digital subtraction angiography (DSA), Duplex Ultrasound, Magnetic Resonance Angiography (MRA) and computerized tomographic angiography [11]. Intra-arterial DSA is considered as the most accurate method for the anatomical detection of RAS but its usability is hindered by its invasive nature and the complications which arise while assessing the pathophysiological significance of the atherosclerotic lesions. They are also known to be prone to inter observer variation [12]. Nuclear medicine and Ultrasonography, though non-invasive in nature, fail to provide information regarding the location and the degree of stenosis of the RAS [13, 14]. Alternatives to these methods include MRA and CTA which are well equipped for angiographic illustration to assess the flow through the renal artery in the case of a stenosis. These methods when coupled with DSA, which is used as a reference is known to be more accurate than in detecting and analysing atherosclerosis than ultrasonographic techniques [15]. However, longer study times susceptible to user errors and difficulty in ascertaining the narrowing of the arteries in patients with severe kidney-related problems are some of the limitations of these methods [16].

In such circumstances, use of Computational Fluid Dynamics (CFD) in conjunction with MRA or CTA data can increase the accuracy in analysing the flow patterns in complex patient-specific arterial geometries. CFD is a powerful tool which makes use of different numerical methods and algorithms and has been increasingly used by researchers lately in applications pertaining to cardiovascular diseases. Various studies have used it to model and analyse different arteries in the

cardiovascular systems i.e., coronary arteries, carotid arteries and renal arteries; in both healthy and pathologic conditions [17-19]. Feasibility of its use in analysing pathological arteries from the data based on MRA slices was also tested. It proved to be a useful tool for non-invasive investigation of RAS [20]. The relation between geometric factors such as eccentricity of the stenosis and its severity on the blood flow was investigated. The parameter in question was pressure difference across the stenosed region which was established to have no dependency on the eccentricity of the stenosis [21].

Analysis of blood flow in the thoracic aorta and its peripheral branches i.e., the renal arteries, the iliac arteries, the celiac artery and the super mesenteric artery was done by observing wall shear stress (WSS) to locate potential sites where recirculation might occur. The region of bifurcation of the renal arteries tended to be the location of plaque formation which was the case both experimentally and clinically [22, 23]. Regions of flow separation where the flow led to an artery with smaller diameter was sensitive to recirculation those regions were flow led to arteries of larger diameter. The use of CFD in accurately evaluating the severity of RAS in pathological arteries was demonstrated in [24]. Numerical methods used to capture the turbulence of the flow was pivotal in the haemodynamic characterisation of the biologically realistic models before the growth of atherosclerotic plaque and after stent implantation due to severe stenosis formation. Therefore, as computational capabilities improve over time, the role of CFD can be integrated with everyday clinical practice, aiding the clinician in the diagnosis of these conditions.

Even though there are several numerical studies, analysing the haemodynamic of RAS, however the effect of branching angle in renal artery vasculature is limited. Hence in the present study, CFD simulation was used to analyse the effect of angulation on arterial pathology, with different stenosis grade present on both the renal arteries. The branching angles considered for this study ranged from 30° to 90° along the abdominal aortal axis. Flow through normal renal arteries of similar angulation was used as a means of comparison to gauge the severity of the stenosis. All the models adopted for this numerical study were idealistic in its vasculature for both the abdominal aorta and the renal arteries. Simplification of the models was necessary as finite element methods compounded by coupled parameters, are computationally restrictive to some extent [25].

Therefore, simplification of the renal system was sought for in this study. Parameters used to examine the flow were time-averaged velocity (TAV), pressure difference, mass flow rate, time-averaged wall shear stress (TAWSS) and virtual fractional flow reserve (vFFR). These variables have been closely related to progression of atherosclerosis and RAS [26]. Velocity and pressure difference are important parameters with which potential sites of flow recirculation. Monitoring the fluctuations of WSS over time remains crucial in understanding the effect of flow on the endothelium. Lastly, vFFR presents itself as a viable alternative to invasive FFR in anatomical evaluation of pathological arteries by quantifying the extent of blood flow through an artery.

The current study compares the flow behaviour through stenosed, renal arteries of two different grades on either branch to investigate the changes in haemodynamic behaviour by virtue of the branching angle of the renal artery.

## 2. Methodology

### 2.1. Theory

The simulation of blood flow in the abdominal aorta-renal artery systems is done with the conjecture that the flow of blood is Newtonian, incompressible and laminar [27, 28]. The governing equation used are the continuity and the incompressible Navier-Stokes equation shown in Eqs. (1) and (2) [29].

$$\nabla . v = 0 \tag{1}$$

$$\rho \left( \frac{\partial v}{\partial t} + v \nabla v \right) = -\nabla p + \mu \nabla^2 v \tag{2}$$

In the above equation, $v$ represents flow velocity, $\rho$ is the density and $\mu$ represents the dynamic viscosity of blood. The notation p refers to the pressure of the system.

### 2.2. Modelling and analysis

The fluid domains analysed in the present study is the abdominal aorta-renal artery junction, with the renal arteries bifurcating at various angles along the flow direction. Five models of the abdominal aorta-renal artery system with angulation ranging from 30° to 90° taken at regular intervals of 15° were considered. These models are referred herein as Artery-30, Artery-45, Artery-60, Artery-75 and Artery-90, the suffix indicating the bifurcating angles of the symmetric renal artery systems. Firstly, standard computerized tomography-angio slices of the renal artery system were obtained, which were subjected to reconstruction using the Materialize MIMICS software tool [30].

The reconstructed models were defeaturized using the CATIA V5 R19 computer-aided design tool [31]. Picturised representation of the steps involved in reconstruction and defeaturization is shown in Fig. 1. The first step depicts reconstruction of the geometry whereas the second and third step portray the process of defeaturization. The simplification and defeaturization is done in such a way that the accuracy of the model isn't affected i.e., by keeping the average diameter of each of the aorta and arteries unchanged. The aortal and renal diameter along with the location of the Ostia remains same. Geometrical simplification of the models enables to analyse blood flow in idealized conditions where only a single factor can cause changes in blood circulation i.e., the angle of bifurcation of the renal arteries.

Figure 2 depicts the different regions of the two types of artery models which were examined: healthy and stenosed. Region-1 represents the upper portion and region-3, the lower portion of the abdominal aorta. Region-2 and 4 illustrate the right and the left symmetrical renal arteries respectively. Region-4 and 5 which are exclusive only to the stenosed artery models, represent the stenosed-right and the stenosed-left artery respectively. The right renal artery consisted of a stenosis with a degree in between 75-80% by diameter, with the stenosed diameter, 0.225 times the original renal diameter. The stenosis is asymmetrical to the renal artery axis, with an offset of 0.228 mm. The left renal artery consists of a symmetrical stenosis degree in between 80-85%, with the stenosed diameter, 0.18 times the original diameter. The regions of stenosis where virtually generated, wherein the right renal artery contained a non-critical stenosis and the left artery, a critical stenosis. Several

studies have indicated that renal artery stenosis above the threshold of 80% is considered as critical and calls for immediate treatment [32, 33].

Grid dependency tests were carried out prior to the simulations, wherein the velocity parameter was monitored at different sections of both the normal and stenosed artery models. Figure 3 illustrates the sections used in the stenosed Artery-60 model. Simulations were conducted under steady state conditions for meshes of varying number of elements, the procedure like the one done in [34]. Static velocity value of 0.245 m/s; which is the early systolic velocity and a static pressure of 90 mmHg; the lower limit of blood pressure at resting conditions. A mesh comprising of structured octahedral and hexahedral elements was used in this study as depicted in Fig. 4. Poly-Hexcore mesh as it is known in the FLUENT 19 meshing software, comprises of octahedral elements at the periphery and hexahedral elements at the interior.

By incorporating mosaic technology, different types of meshes are automatically connected with polyhedral element, thereby filling the region with hexahedral elements [35]. This is known to make the mesh computationally efficient, increase the accuracy and decrease the simulation time of the solution [36]. Figures 5 and 6 depict the variation in the velocities through the four different sections for the normal and stenosed Artery-60 model. It is inferred from the velocity distribution graphs that meshed models of normal renal artery achieved stabilization after 370000 elements whereas that of stenosed arteries normalized after 400000 elements. The respective number of elements were considered for the final mesh, with which the simulation was done.

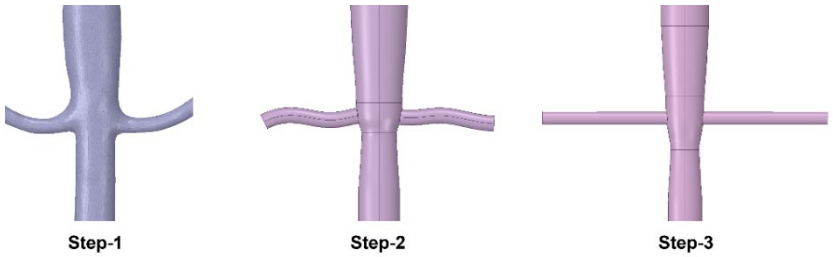


**Fig.1. Steps involved in reconstruction and defeaturization of the normal Artery-90 mode.**

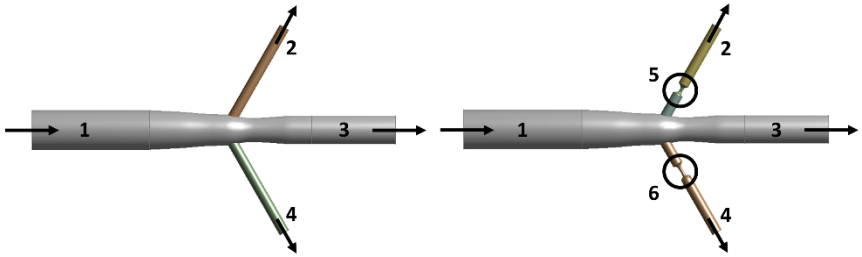


**Fig. 2. Geometric description of CFD model with normal and stenosed renal arteries of Artery-60.**

In the present study, the artery models, both normal and stenosed were solved using FLUENT Solver 19.0 under time varying conditions. Considering the pulsatile nature of blood flow in the body, time varying velocity inlet and pressure outlet conditions were translated into a user-defined function and applied to the solver [34, 37]. Figure 7 shows the pulsatile velocity and pressure profiles taken as the inlet and the outlet boundary conditions respectively. The outer wall of the abdominal aorta and the renal artery was rigid body devoid of deformation [38]. This is a common assumption which can be taken considering the presence of atherosclerotic lesions on the arterial wall. Properties of blood; density and molecular viscosity was taken as 1050 kg/m$^3$ and 0.00345 Pa-s respectively [39]. The assumption of blood being considered as a Newtonian fluid is valid for blood vessels large enough, when compared to the size of a red blood cell [18]. The SIMPLE formulation technique was used as a method of conducting the analysis with residual values of $1x10^{-5}$ as the convergence criteria in order to increase the accuracy of the obtained solution [40]. Implicit formulation was employed with no restrictions placed in grid and time-step size. The entire simulation run-time was taken to be 0.9 s as it is the duration of a single pulse under resting conditions of the body [41]. Time dependent tests revealed 0.005 s as the adequate size of each time-step, with 180 being the total number of time steps. The results obtained from the analysis of normal and stenosed renal arteries can aid us in posturizing the effects of angulation as well as the presence of critical and non-critical stenosis on the functioning of the renal system.

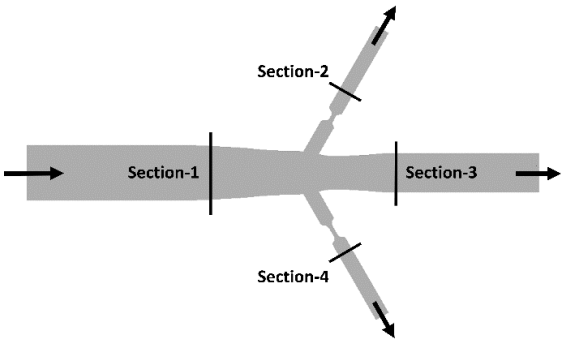


**Fig. 3. Sections used to monitor the parameters in stenosed Artery-60 model for the grid dependency test.**

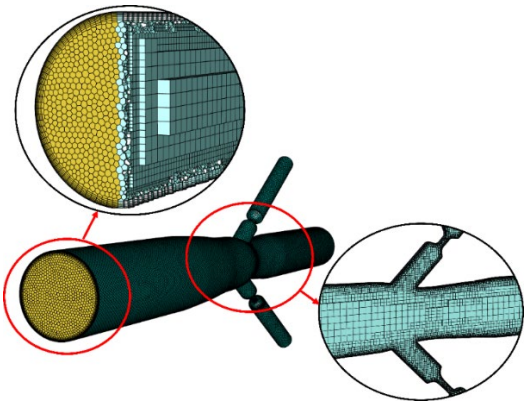

**Fig. 4. Detailed surface and sectioned view of the Poly-Hexcore mesh of the stenosed Artery-60 model.**

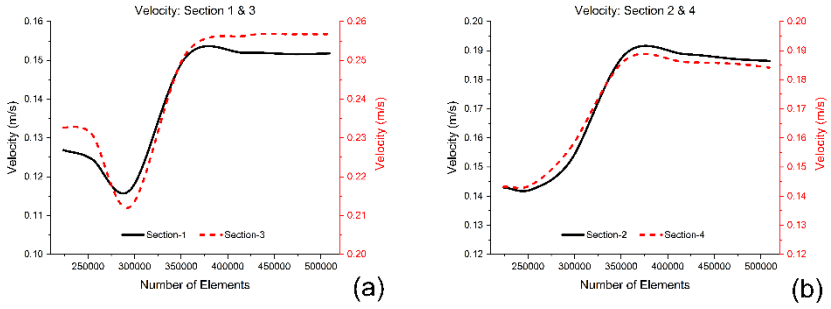


**Fig. 5. Velocity Comparison in different elements at various sections of the normal Artery-60 model.**

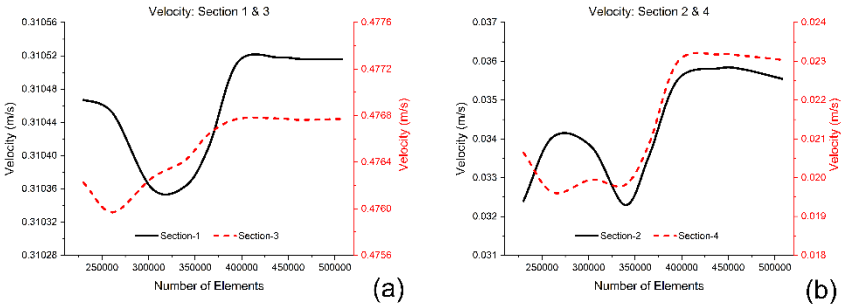


**Fig. 6. Velocity Comparison in different elements at various sections of the normal Artery-75 model.**

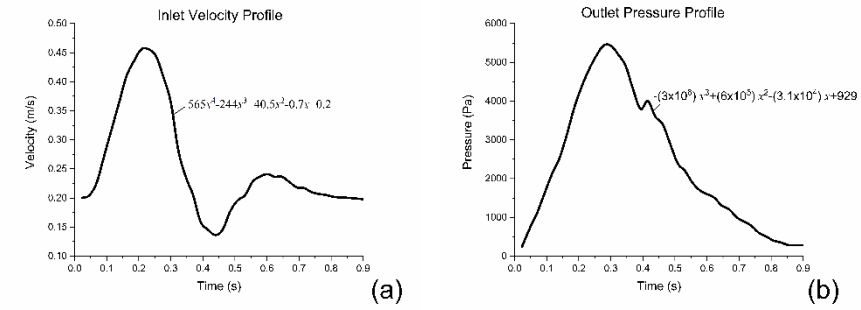


**Fig. 7. Pulsatile wave pattern a) Velocity wave at inlet; and b) Pressure profiles at outlet.**

## 3. Results and Discussions

Ten models of renal artery, five each of which were normal and stenosed on both renal arteries of different angulations with respect to the abdominal aorta were subjected to numerical analysis under transient conditions. The parameters observed were TAV, pressure difference (PD), mass flow rate (MFR), TAWSS and FFR of a

renal artery model. Analysing velocity helps in ascertaining the extent of flow recirculation in the blood flow [42]. TAWSS is an essential parameter in estimating the probability of thickening of the arterial walls [43]. Finally, FFR acts a prospectus in providing a quantitative value for variation in blood flow between the different artery models [44]. The results obtained were observed at regular intervals of time and extracted either in the form of contour plots or Cartesian charts.

## 3.1. Time-averaged velocity

Time-averaged velocity (TAV) parameter as the name suggests representing the velocity magnitude averaged over a period of time *T*. By averaging the parameter with time, the effects due to the cardiac cycle is seen rather than at specific points in time. This provides a realistic scenario when comparing the haemodynamic between models of different angulation. The equation for this variable is given in the equation below:

$$Time - Averaged\ Velocity = \frac{1}{T}\int_0^T \left(|v_x| + |v_y| + |v_z|\right) dt \quad (3)$$

where, $v_x$, $v_y$ and $v_z$ are the velocity values in the *x, y* and *z* directions respectively.

Figure 8 shows the velocity contour plot of all the normal abdominal aorta-renal artery models averaged over time $T = 0.9$ s. Blood flow is similar in either of the normal renal arteries of all angulations, given the symmetric nature of the models. Flow is similar in the abdominal aorta, with changes seen only in the region of branching of the renal arteries. Separation of blood flow is known to cause a region of flow recirculation at the proximal wall of the renal artery near the region of the Ostia [22]. The size of the recirculation zone and the extent of eddy formation varied between artery models of different angulation [42].

Renal arteries with higher angulation i.e., Artery-60, Artery-75 and Artery-90 saw greater flow recirculation due to flow impingement on the distal wall. The velocity contours of the stenosed arteries are shown in Fig. 9. The variation in the velocity parameter is significant because of angulation and stenosis. The flow is characterized by the presence of a jet at the throat of the stenosis [34]. Flow is mostly similar with minor variations because of non-identical regions of stenosis on either artery. In Artery-30, the extent of the flow jet is minimal, with lower velocities observed at the throat. As seen from the image, blood flows along the curvature of a region of the distal wall prior to the stenosis. Presence of recirculation is also observed at the Ostia and at the infrarenal region of the abdominal aorta. Progression of the fluid jet and the initiation of flow impetus on the distal wall were some of the observations realized in Artery-45. Artery-60, Artery-75 and Artery-90 showed similar behaviour albeit with increasing lengths of the flow jet, higher velocities at the throat and sharper impinge of the fluid on the distal wall near the Ostia.

In normal arteries, velocity was found to decrease with increase in angulation, but it was the opposite for stenosed arteries. The artery with higher degree of stenosis i.e., the left renal artery experienced higher velocities compared to the right renal artery which had a non-critical stenosis (< 70% reduction in diameter) [20]. The common site for recirculation and development of atherosclerotic lesions in normal renal arteries are known to be at the Ostia [22]; a flow behaviour curtained

in the Ostia of stenosed arteries. Low velocities near the distal wall were observed in stenosed arteries at a higher renal angle, which were also subjected to change in direction throughout the duration of the pulsatile flow. These occurrences tend to precede consistent progression of atherosclerotic plaques [23].

Additionally, changes in velocity at the wall have also led to variation in shear stresses, effecting the mass transfer between the fluid medium and the endothelium [43]. In such cases, by virtue of its geometry, pathological arteries at a higher branching angle ($\geq 60°$ ) with non-critical stenosis would progress to a critical stage, and the presence of an existing higher stenosis grade, would lead to ischemic nephropathy. The results obtained was analogous to the observations done in the numerical study [22, 34], wherein the disparity in WSS distribution between the proximal and distal wall was discovered. These observations also coincided with the findings from an experimental study done in [23], wherein the effect of low velocities leading to lower wall shear stresses at the bifurcation regions in arteries were contemplated. TAV presents a more pragmatic approach in analysing the flow behaviour throughout the pulse cycle.

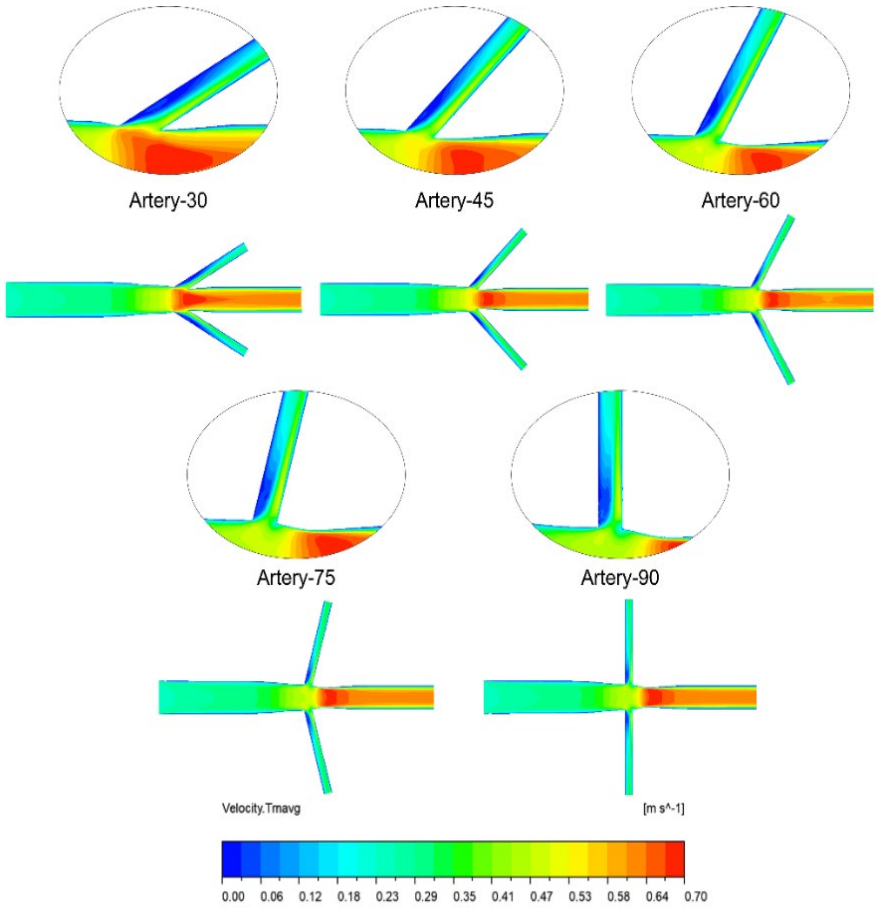


**Fig. 8. Transient-average velocity contour plot of normal artery models of all angulations.**

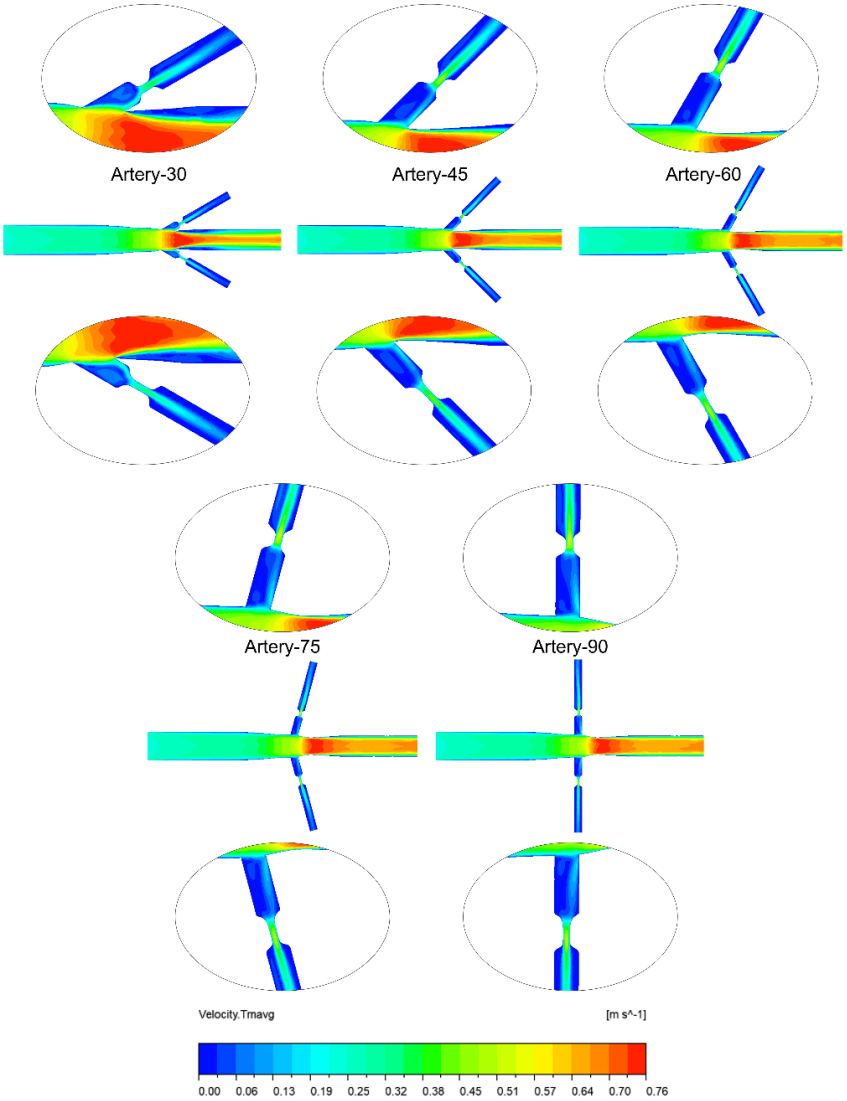


**Fig. 9. Transient-average velocity contour plot of normal artery models of all angulations.**

## 3.2. Pressure difference and mass flow rate

A better understanding of the velocity parameter can be obtained from observing and correlating it with the changes observed in pressure difference (PD) and mass flow rate (MFR). Figure 10 illustrates the points and cross sections used to note down these parameters. The respective points were taken at equal distances from the centre of the throat of the stenosed region. The expressions, $(R_d - R_p)$ and $(L_d - L_p)$ gives the PG at the right and left stenosed arteries respectively. Circular cross sections at halfway point of either of the renal arteries post the stenosed region, were generated to calculate the average MFR. Similar steps were carried out for normal arteries for comparison.

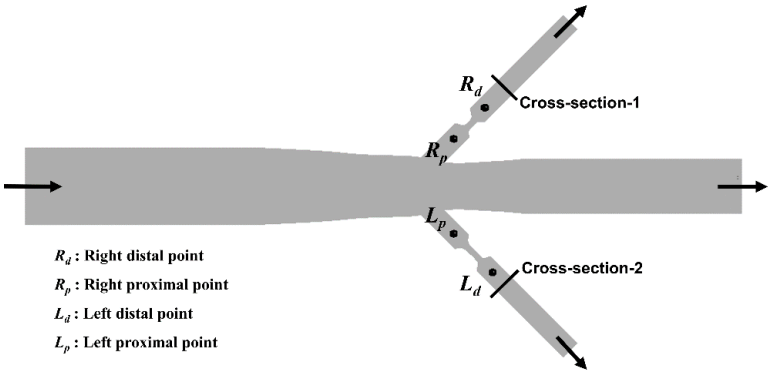


**Fig. 10. Points and cross-sections utilized for observing PD and MFR.**

The variation of pressure difference in the renal artery with angulation ranging from 30° to 90° is given in Figs. 11(a) to 15(a) accordingly. The peaks represent negative pressure gradient (reverse flow) whereas the troughs represent positive pressure gradient (normal flow). Healthy renal arteries had the PD across two points in the renal artery under the normal physiological values, portrayed by the relatively flat curves in Figs. 11(a) to 15(a). But in the case of stenosed arteries, the difference was significantly higher than the normal cases [29]. As seen from the graphs, increase in branching angle tended to exaggerate the PD, increasing the difference across the region of stenosis. Moreover, degree of stenosis too affected the pressure parameter as the left renal artery with a higher stenosis grade experienced greater gradient than the left [20]. Significant oscillations were observed at peak systole, peak diastole and late diastole characterized by the sharp peaks and troughs. Maximum value of PD was observed at peak systole [34]. In these phases of the cardiac cycle, the pressure gradient in the left renal artery was approximately twice the value noted at the right renal artery for all renal angulations. Quantitatively, the difference in pressure in the right renal artery varied from 800 Pa (6 mmHg) to 1300 Pa (9.75 mmHg) whereas PD in the right renal artery, it ranged from 1375 Pa (10.3 mmHg) to 2000 Pa (15 mmHg) as the renal angle increased.

Figures 11(b) to 15(b) illustrates the changes in MFR throughout the cardiac cycle for models Artery-30 to Artery-90. MFR unlike the velocity parameter, tended to decrease with the presence of stenosis, with higher degree of stenosis offering more flow resistance [20]. In normal arteries, variation of the MFR curve was similar to that of the waveform of inlet velocity given in Fig. 7(a), with optimal flow rate occurring at peak systole, reduced rate at peak diastole and intermediate flow at late diastole. The presence of stenosis drastically decreases the flow rate, to such an extent that the minimum flow rate observed at peak diastole was roughly greater than the maximum flow rate noted throughout the cycle in stenosed arteries. Lower mass transfers have always been linked with development of atherosclerotic plaques and increase in blood pressure [23]. MFR curves of stenosed Artery-30 show minimal oscillations compared to the other artery models, which shows that the flow recirculation observed (in Fig. 9 at the proximal wall preceding the stenosed region), to be weak and inconsequential to the progression of RAS [6].

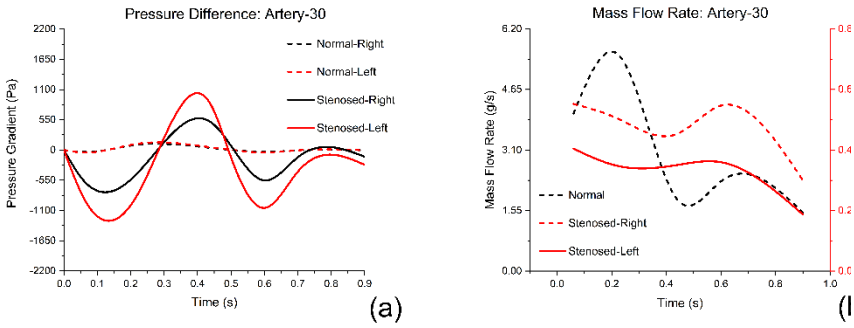


**Fig. 11. Transient (a) PD; and (b) MFR for Artery-30.**

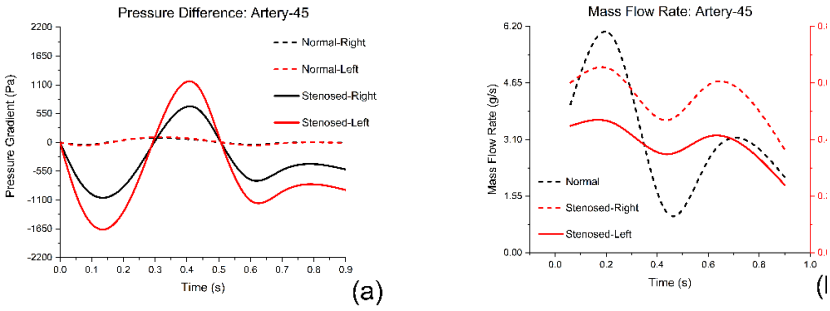


**Fig. 12. Transient (a) PD; and (b) MFR for Artery-45.**

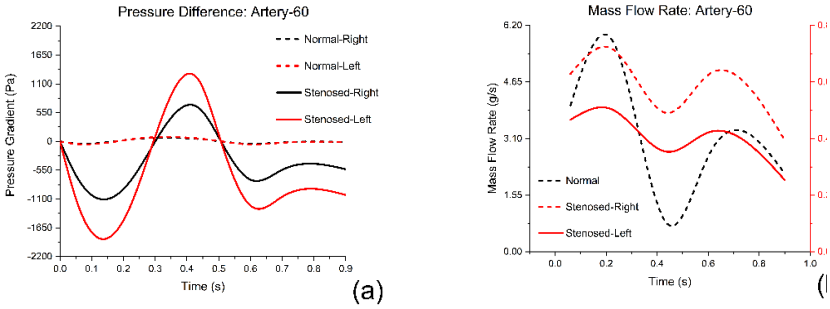


**Fig. 13. Transient (a) PD; and (b) MFR for Artery-60.**

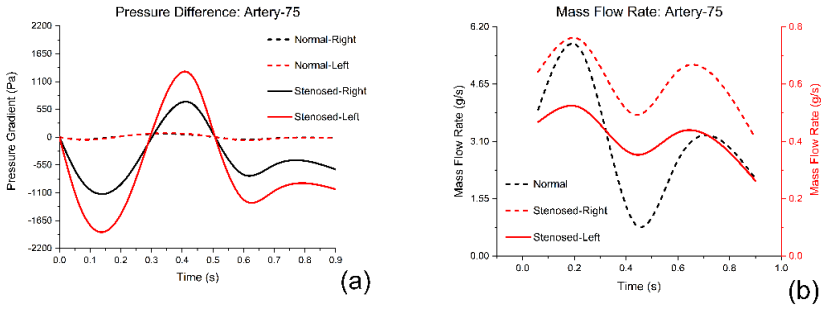


**Fig. 14. Transient (a) PD; and (b) MFR for Artery-75.**

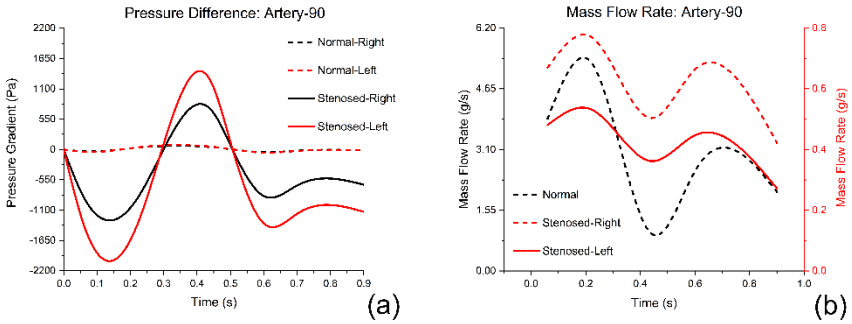


**Fig. 15. Transient (a) PD; and (b) MFR for Artery-90.**

The variation in pressure gradient with respect to time as shown in the above graphs, aids in understanding the physiological significance of a given atherosclerotic lesion [3]. It has always been associated with the direction of blood flow; higher the magnitude of oscillations, greater is the extent of reversed flow, when large enough is believed to cause flow separation [8]. The presence of stenosis causes oscillation in the PD with the average pressure losses in the left renal arteries of all angulations were noted to be above 10 mmHg. This causes malfunction in the renin-angiotensin-aldosterone system (RAAS), which is known to cause renal hypertension [45]. Therefore, patients with arterial vasculature at higher angulations have more chances of getting diagnosed with hypertension, in the event of severe plaque formation. Such variations help the clinicians in formulate certain treatment plans. The observations noted regarding pressure losses are consistent with [21], wherein a threshold pressure of 10 mmHg was observed in arteries of larger renal angles, having stenosis ranging between 75-80%. Correlation of mass flow rate results were also done with [20] and was found to be coherent with respect to the MFR values corresponding to different grades of stenosis.

### 3.3. Time-averaged wall shear stress

Time-averaged wall shear stress (TAWSS) is a function of wall shear stress (WSS) averaged over the entire time *T*. The expression for the parameter is given in the equation below.

$$TAWSS = \frac{1}{T}\int_0^T \left(|WSS_x| + |WSS_y| + |WSS_z|\right) dt \quad (4)$$

where, $WSS_x$, $WSS_y$ and $WSS_z$ are the WSS values resolved at *x, y* and *z* directions respectively.

Figure 16 exhibits the WSS contours of all the normal artery models at five different angulations averaged over the entire time duration of 0.9 s. Shear stress along the length of the abdominal aorta increased till the region of bifurcation, where it is highest and lowered further upstream [34]. In normal renal arteries, the distal walls experienced higher amounts of stress compared to that of proximal walls [7]; the values of shear stress decreasing as the bifurcation angle of the renal artery increased. As mentioned earlier, arteries of higher angulation experience a higher impetus when the flow impinges on its distal walls. Therefore, the overall area in which the shear stress was distributed across was also higher for higher

angulated arteries [8]. TAWSS plots of the stenosed arteries illustrated in Fig. 17, showed contrasting trends compared to the normal ones. For renal arteries of lower angulation i.e., Artery-30 and Artery-45, the maximum TAWSS was found at the distal wall at the region of branching. In the rest of the models, the maximal value was seen at the throat of the stenosis; about 2 Pa higher than the peak value observed in the normal arteries. The value of TAWSS at the throat tended to increase with angulation. TAWSS behaviour at the region of bifurcation in the distal side is like the case of normal arteries, wherein higher angulated arteries experienced minimal stress in the said region.

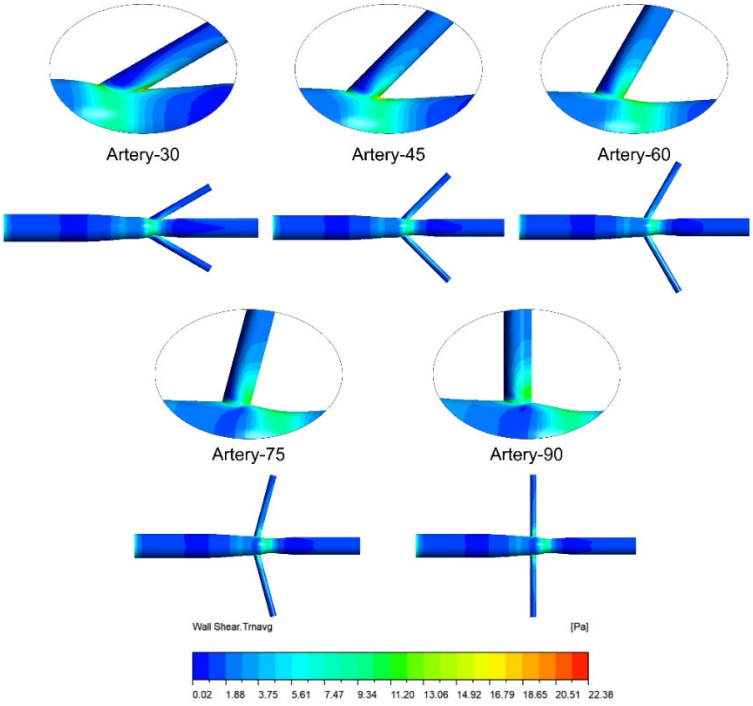


**Fig. 16. TAWSS contours for normal artery models.**

TAWSS is an appropriate parameter with which localized transport phenomena between the components of the blood stream and the arterial intima can be carefully examined upon [46]. Momentary changes in certain phases of the cardiac cycles tend to be insignificant in varying the TAWSS parameter. Under these circumstances, the haemodynamic behaviour on a larger scale in time can be examined, as the duration of the development of plaque formation associated with atherosclerosis is known to be considerably long [26]. Distribution of shear stress on the arterial walls have always been linked with atherogenesis [27]. It is a very sensitive parameter as minimal changes in the shear stress value can have significant implications in the flow behaviour. Areas of low shear stress distributions like the proximal wall of the renal artery, are known to be sites of flow recirculation, which is linked to the onset of plaque formation [17]. Higher amounts of shear stress either at the throat of the stenosis or in areas subjected to incoming flow impingement at the junction such as the distal wall, often cause shear thinning in said regions and other regions downstream [8]. Elevated TAWSS has been linked

to the increase in permeability of the endothelial cells leading to its deterioration. Moreover, this can cause rupturing of the plaque prompting the formation of clots, thereby deterring the flow completely [47]. From the Fig. 17, the role played by geometry in influencing the TAWSS behaviour is clearly seen, with renal arteries at a higher angulation experiencing more spatial shear stress oscillations, thereby increasing the atherogenic haemodynamic stress on such vasculature.

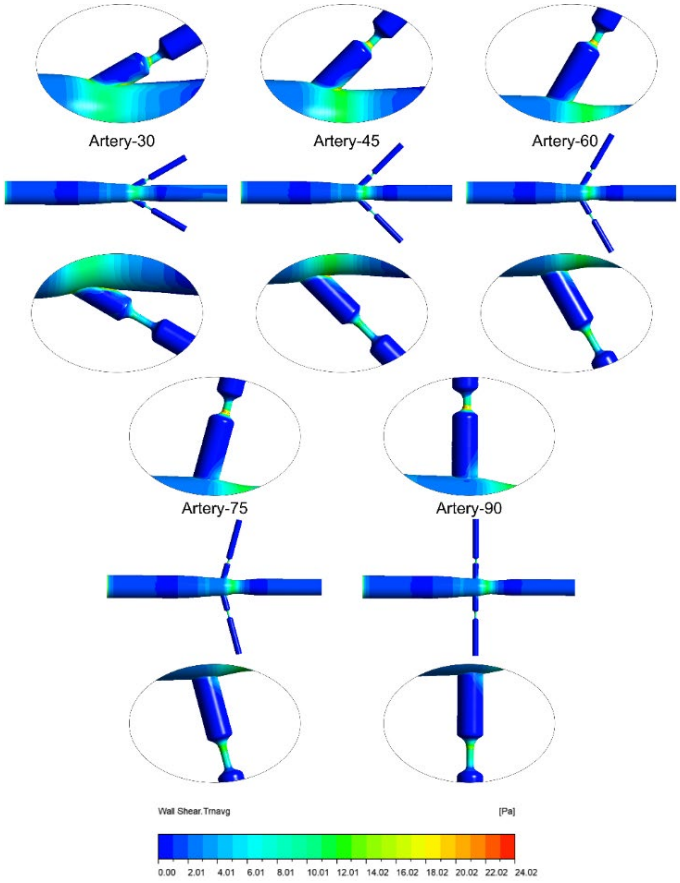


**Fig. 17. TAWSS contours for stenosed artery models.**

## 3.4. Virtual fractional flow reserve

Fractional flow reserve (FFR) is defined as a value which quantifies the degree of blockage in a stenosed artery. This can also be defined as the ratio of maximum achievable of blood flow through a region of arterial stenosis to the maximum possible blood flow through the same region in the absence of stenosis. The equation for FFR is expressed as the following [44].

$$Fractional\ flow\ reserve = P_d/P_p \tag{5}$$

The term $P_d$ and $P_p$ refers to the maximum pressure at a point distal and proximal to the region of stenosis respectively. It is calculated virtually using two equidistant points across the region of stenosis; the points as illustrated in Fig.

10, as is the case in [48], hence the name virtual fractional flow reserve (vFFR). By calculating this value, it is possible to distinguish every stenosed artery model based on the severity of a critical and non-critical stenosis. Table 1 presents the values of the FFR for each renal artery of different angulation and of different cases of stenosis.

**Table 1. vFFR values of the artery models.**

| Virtual Fractional Flow Reserve Values | | | |
|---|---|---|---|
| | **Normal Artery** | **Stenosed Right Artery (75-80% Stenosis)** | **Stenosed Left Artery (80-85% Stenosis)** |
| Artery-30 | 1.004 | 0.896 | 0.820 |
| Artery-45 | 1.001 | 0.849 | 0.772 |
| Artery-60 | 0.999 | 0.834 | 0.756 |
| Artery-75 | 0.999 | 0.829 | 0.751 |
| Artery-90 | 0.999 | 0.828 | 0.749 |

As seen from the above given table, the FFR values are calculated for the stenosed right and left artery and compared with that of the normal one. The normal arteries all have an approximate value of 1 due to the absence of any deterrent to the flow. However significant variations were noted in the case of the right and left stenosed arteries. Increase in renal artery angulation saw decrease in FFR values symbolizing reduced blood flow to the kidneys. In the case of the right renal artery with a stenosis of 75-80%, the percentage of blockage reduced from 10.4% to 17.2%, with a net increase of 6.8%, as the angulation increased. Reduction in blood flow in the left renal artery, which had a stenosis of 80-85%, was observed with a blockage of 18% for renal artery with 30° branching to 25.1% for the one with 90° branching. The increase in the reduction of blood flow was 7.1%, like the right renal artery. Though the increase in blockage is the same in both cases, the extent of impediment is severe in the case of the left renal artery. The above results are a clear indication about the influence of geometry in determining the blood flow, although the respective arteries have the same degree of stenosis in their given ranges.

Fractional flow reserve is a lesion specific quantity, which isn't contingent on the aortic pressure, unlike trans-stenotic pressure. It enables in assessing the severity of a stenosis and provides insights on the condition of the surrounding vasculature [19]. According to clinical trials done on renal artery stenosis, cases with FFR values greater than 0.8 were classified as non-ischemia producing stenosis, which was then prescribed to medical treatment. Some studies have also associated the release of renin in the renal system in conditions where the FFR value was below 0.9 [48]. FFR values greater lesser than 0.75 or in transition zone between 0.8 and 0.75 are considered as ischemia producing stenosis [44]. Left renal arteries with 45°, 60° and 75° angulation all fall under the transition zone whereas the artery with 90° falls below the threshold. As the angulation of the renal arteries increased, the stoppage of blood flow also increased, transitioning from a non-severe case to a severe one. In the present case, the stenosis in the right renal artery was considered to have significant RAS but not in need of revascularization procedures. In the case of right renal artery with branch angle above 45°, the chances of ischemic nephropathy were relatively high. Under these circumstances, surgical revascularization using balloon angioplasty or use of an angiotensin converting enzyme (ACE) inhibitors would be adopted [1].

## 4. Conclusions

This study presents a case for the possible use of CFD in routine clinical diagnosis to assess the pathological renal arteries. The current study compared the flow behaviour through stenosed, idealistic renal arteries of two different grades by diameter (75-80% and 80-85%) on either branch to investigate the changes in haemodynamic behaviour by virtue of the branching angle of the renal artery. Simulations were carried out in arteries of five different renal angles, ranging from 30° to 90° at frequent steps of 15°. The variables monitored to examine the flow characteristics were TAV, PD across the region of stenosis, mass flow rate to the kidney, TAWSS and vFFR.

- Comparatively longer timescales related to the development of the atherosclerotic lesions necessitates time-averaged parameters like TAV and TAWSS. Observation of TAV showed significant changes in the distinctively angled arteries.
- In contrast to normal artery of identical angulation, a stenosed artery had blood flow at higher velocity, along with the formation of a flow jet at the throat; higher grade stenosis tends to have greater velocities. Similar velocity patterns influence the exaggeration as the bifurcation angle increases.
- Analysing the pressure gradients across the stenosis region observed increased amounts of pressure loss. Higher stenosis grades and larger renal artery angulations tends to have larger pressure oscillations.
- MFR to the kidney reduced significantly due to the presence of stenosis; the right renal artery having a flow rate 30% more than the left renal artery, with Artery-30 having marginally higher flow rates.
- TAWSS provided a clear depiction on the effect of angulation on flow separation, flow recirculation and shear thinning. Stenosed arteries had higher values of shear stress at the stenosis throat, which increases with the higher angulation of the renal artery. In arteries of higher renal angle i.e. above 45°, this would lead to shear thinning of arterial walls downstream and lead to plaque rupture, resulting in clot formation.
- The severity of these stenosis coupled with the branch angle was highlighted using virtual FFR values calculated using the maximum pressure values at two equidistant points across the region of stenosis. For a renal artery with the same grade of stenosis, variation in the branching angle was observed to cause changes in hyperaemic flow, with maximum blockage of 18% and 25% calculated in the right and left renal artery accordingly. Based on the vFFR values stenosis in the right renal artery at all angulations were classified as non-ischemia causing cases though they are significant RAS.
- In the case of the left stenosed arteries of stenosis greater than 80% by diameter, having a bifurcating angle greater than 45° resulted in severe blockage, and would possibly lead to ischemic nephropathy. For patients with critical stenosis at such vasculatures, surgical revascularization methods would be the appropriate method for treatment.
- The results stressed on the influence of a geometric feature-bifurcating angle at the abdominal aorta-renal artery junction affected the flow behaviour and its consequences in pathological renal arteries of different grades of stenosis.

- With CFD analysis approach it is possible to assess the pathological arteries non-invasively. Further, such studies can be useful in clinical diagnosis.

## Nomenclatures

| | |
|---|---|
| $p$ | Pressure of the fluid system, Pa |
| $t$ | Time, s |

### *Greek Symbols*

| | |
|---|---|
| $\rho$ | Constant flow density (1050 kg/m$^3$) |
| $\upsilon$ | Velocity vector |
| $\mu$ | Dynamic Viscosity (0.00345 Pa-s) |

### Notations and Abbreviations

| | |
|---|---|
| Artery-30 | Renal Artery with 30° angulation to the abdominal aorta |
| Artery-45 | Renal Artery with 45° angulation to the abdominal aorta |
| Artery-60 | Renal Artery with 60° angulation to the abdominal aorta |
| Artery-75 | Renal Artery with 75° angulation to the abdominal aorta |
| Artery-90 | Renal Artery with 90° angulation to the abdominal aorta |
| CFD | Computational Fluid Dynamics |
| CTA | Computerised Tomography-Angiography |
| DSA | Digital Subtraction Angiography |
| MFR | Mass Flow Rate |
| MRA | Magnetic Resonance Angiography |
| PD | Pressure Difference |
| RAS | Renal Artery Stenosis |
| TAV | Time-Averaged Velocity |
| TAWSS | Time-Averaged Wall Shear Stress |
| vFFR | Virtual Fractional Flow Reserve |

## References

1. Safian, R.D.; and Textor, S.C. (2001). Renal-artery stenosis. *New England Journal of Medicine*, 344(6), 431-442.
2. Mann, S.J.; and Pickering, T.G. (1992). Detection of renovascular hypertension. *Annals of Internal Medicine*, 117(10), 845.
3. Olin, J.W. (2002). Atherosclerotic renal artery disease. *Cardiology Clinics*, 20(4), 547-562.
4. Derkx, F.; and Schalekamp, M. (1994). Renal artery stenosis and hypertension. *The Lancet*, 344(8917), 237-239.
5. Ollivier, R.; Boulmier, D.; Veillard, D.; Leurent, G.; Mock, S.; Bedossa, M.; and LeBreton, H. (2009). Frequency and predictors of renal artery stenosis in patients with coronary artery disease. *Cardiovascular Revascularization Medicine*, 10(1), 23-29.
6. Friedman, M.; Deters, O.; Mark, F.; Brentbargeron, C.; and Hutchins, G. (1983). Arterial geometry affects hemodynamic *1A potential risk factor for atherosclerosis. *Atherosclerosis*, 46(2), 225-231.

7. Miranda, A.I.; Oliveira, P.J.; and Pinho, F.T.D. (2008). Steady and unsteady laminar flows of Newtonian and generalized Newtonian fluids in a planar T‐junction. *International Journal for Numerical Methods in Fluids*, 57(3), 295-328.
8. Cho, Y.I.; Back, L.H.; and Crawford, D.W. (1985). Experimental investigation of branch flow ratio, angle, and Reynolds number effects on the pressure and flow fields in arterial branch models. *Journal of Biomechanical Engineering*, 107(3), 257-267.
9. Chandler, A.B. (1978). *The thrombotic process in atherogenesis*. New York: Plenum Publishing Cooperation.
10. Myers, J.G.; Moore, J.A.; Ojha, M.; Johnston, K.W.; and Ethier, C.R. (2001). Factors influencing blood flow patterns in the human right coronary artery. *Annals of Biomedical Engineering*, 29(2), 109-120.
11. Rountas, C.; Vlychou, M.; Vassiou, K.; Liakopoulos, V.; Kapsalaki, E.; Koukoulis, G.; and Stefanidis, I. (2007). Imaging modalities for renal artery stenosis in suspected renovascular hypertension: prospective intraindividual comparison of colour doppler US, CT angiography, GD-enhanced MR angiography, and digital subtraction angiography. *Renal Failure*, 29(3), 295-302.
12. Schreij, G.; de Haan, M.W.; Oei, T.K.; Koster, D.; and de Leeuw, P.W. (1999). Interpretation of renal angiography by radiologists. *Journal of Hypertension*, 17(12), 1737-1741.
13. Itoh, K. (2001). 99mTc-MAG3: Review of pharmacokinetics, clinical application to renal diseases and quantification of renal function. *Annals of Nuclear Medicine*, 15(3), 179-190.
14. Li, J.; Jiang, Y.; Zhang, S.; Wang, L.; Ouyang, Y.; and Qi, Z. (2008). Evaluation of renal artery stenosis with hemodynamic parameters of Doppler sonography. *Journal of Vascular Surgery*, 48(2), 323-328.
15. Vasbinder, G.B.C.; Nelemans, P.J.; Kessels, A.G.H.; Kroon, A.A.; de Leeuw, P.W.; and van Engelshoven, J.M.A. (2001). Diagnostic tests for renal artery stenosis in patients suspected of having renovascular hypertension: A meta-analysis. *Annals of Internal Medicine*, 135(6), 401-411.
16. Kwong, R.Y. (2003). Computed tomography scan and magnetic resonance imaging. *Circulation*, 108(15), 104-106.
17. Suo, J.; Oshinski, J.N.; and Giddens, D.P. (2008). Blood flow patterns in the proximal human coronary arteries: Relationship to atherosclerotic plaque occurrence. *Molecular and Cellular Biomechanics*, 5(1), 9-18.
18. Nguyen, K.T.; Clark, C.D.; Chancellor, T.J.; and Papavassiliou, D.V. (2008). Carotid geometry effects on blood flow and on risk for vascular disease. *Journal of Biomechanics*, 41(1), 11-19.
19. Shalman, E.; Barak, C.; Dgany, E.; Noskowitcz, H.; Einav, S.; and Rosenfeld, M. (2001). Pressure-based simultaneous CFR and FFR measurements: understanding the physiology of a stenosed vessel. *Computers in Biology and Medicine*, 31(5), 353-363.
20. Zhang, W.; Qian, Y.; Lin, J.; Lv, P.; Karunanithi, K.; and Zeng, M. (2013). Hemodynamic analysis of renal artery stenosis using computational fluid dynamics technology based on unenhanced steady-state free precession

magnetic resonance angiography: Preliminary results. *The International Journal of Cardiovascular Imaging*, 30(2), 367-375.

21. Heflin, L.A.; Street, C.B.; Papavassiliou, D.V.; and O'Rear, E.A. (2009). A computational investigation of the geometric factors affecting the severity of renal arterial stenoses. *Journal of Biorheology*, 23(2), 102-110.
22. Lee, D.; and Chen, J. (2002). Numerical simulation of steady flow fields in a model of abdominal aorta with its peripheral branches. *Journal of Biomechanics*, 35(8), 1115-1122.
23. Moore, J.E.; and Ku, D.N. (1994). Pulsatile velocity measurements in a model of the human abdominal aorta under resting conditions. *Journal of Biomechanical Engineering*, 116(3), 337-346.
24. Kagadis, G.C.; Skouras, E.D.; Bourantas, G.C.; Paraskeva, C.A.; Katsanos, K.; Karnabatidis, D.; and Nikiforidis, G.C. (2008). Computational representation and hemodynamic characterization of in vivo acquired severe stenotic renal artery geometries using turbulence modelling. *Medical Engineering and Physics*, 30(5), 647-660.
25. Laganà, K.; Balossino, R.; Migliavacca, F.; Pennati, G.; Bove, E.L.; deLeval, M.R.; and Dubini, G. (2005). Multiscale modelling of the cardiovascular system: application to the study of pulmonary and coronary perfusions in the univentricular circulation. *Journal of Biomechanics*, 38(5), 1129-1141.
26. Gessner, F.B. (1973). Brief reviews: Hemodynamic theories of atherogenesis. *Circulation Research*, 33(3), 259-266.
27. Chakravarty, S.; and Sen, S. (2008). Analysis of pulsatile blood flow in constricted bifurcated arteries with vorticity-stream function approach. *Journal of Medical Engineering and Technology*, 32(1), 10-22.
28. Valencia, A.; and Solis, F. (2006). Blood flow dynamics and arterial wall interaction in a saccular aneurysm model of the basilar artery. *Computers and Structures*, 84(21), 1326-1337.
29. Jhunjhunwala, P.; Padole, P.; and Thombre, S. (2015). CFD analysis of pulsatile flow and non-newtonian behavior of blood in arteries. *Molecular and Cellular Biomechanics*, 12(1), 37-47.
30. Shao, H.; Qin, H.; Hou, Y.; Xia, H.; and Zhou, P. (2011). Reconstructing 3D model of carotid artery with mimics and magics. *Advances in Information Technology and Education*, 428-433.
31. Joel, M. E.; and Anburajan, M. (2013, July). 3D modeling of stenotic internal carotid artery treated with stent: A CFD analysis of blood. *In International Conference on Computer, Networks and Communication Engineering (ICCNCE 2013)*. Beijing, China, 148-151.
32. Brink, J.A.; Lim, J.T.; Wang, G.; Heiken, J.P.; Deyoe, L.A.; and Vannier, M.W. (1995). Technical optimization of spiral CT for depiction of renal artery stenosis: in vitro analysis. *Radiology*, 194(1), 157-163.
33. Simon, G. (2000). What is critical renal artery stenosis? Implications for treatment. *American Journal of Hypertension*, 13(11), 1189-1193.
34. Khader, S.M.A.; Azriff, A.; Johny, C.; Pai, R.; Zuber, M.; Ahmad, K.A.; and Ahmad, Z. (2018). Haemodynamics behaviour in normal and stenosed renal artery using computational fluid dynamics. *Journal of Advanced Research in Fluid Mechanics and Thermal Sciences*, 51(1), 80-90.

35. ANSYS Release 19.0 (2019). Documentation, *Mosaic meshing technology*. Canonsburg, PA: ANSYS Inc.
36. Zore, K.; Shah, S.; Stokes, J.; Sasanapuri, B.; and Sharkey, P. (2018). ANSYS CFD study for high lift aircraft configurations. *In 2018 Applied Aerodynamics Conference*. Atlanta, Georgia, 2844.
37. Antiga, L. (2002). *Patient-specific modeling of geometry and blood flow in large arteries*. Ph.d Thesis. Politecnico Di Milano, Dipartimento Di Bioingegneria.
38. Qian, Y.; Takao, H.; Umezu, M.; and Murayama, Y. (2011). Risk analysis of unruptured aneurysms using computational fluid dynamics technology: preliminary results. *American Journal of Neuroradiology*, 32(10), 1948-1955.
39. Zhang, Y.; Sia, S.F.; Morgan, M.K.; and Qian, Y. (2012). Flow resistance analysis of extracranial-to-intracranial (EC-IC) vein bypass. *Journal of biomechanics*, 45(8), 1400-1405.
40. Quemada, D. (1978). Rheology of concentrated disperse systems III. General features of the proposed non-newtonian model. Comparison with experimental data. *Rheologica Acta*, 17(6), 643-653.
41. Tang, B.T.; Cheng, C.P.; Draney, M.T.; Wilson, N.M.; Tsao, P.S.; Herfkens, R.J.; and Taylor, C.A. (2006). Abdominal aortic hemodynamics in young healthy adults at rest and during lower limb exercise: Quantification using image-based computer modeling. *American Journal of Physiology-Heart and Circulatory Physiology*, 291(2), H668-H676.
42. Ameenuddin, M.; and Anand, M. (2018). Effect of angulation and Reynolds number on recirculation at the abdominal aorta-renal artery junction. *Artery Research*, 21, 1-8.
43. Paszkowiak, J.J.; and Dardik, A. (2003). Arterial wall shear stress: Observations from the bench to the bedside. *Vascular and Endovascular Surgery*, 37(1), 47-57.
44. Hill, D.; and Lim, M.J. (2020). *Fractional flow reserve*. In StatPearls. StatPearls Publishing. Retreived Dicember 17, 2020, from https://www.ncbi. nlm. nih. gov/books/NBK482324/
45. Yim, P.J.; Cebral, J.R.; Weaver, A.; Lutz, R.J.; Soto, O.; Vasbinder, G.B.C.; and Choyke, P.L. (2004). Estimation of the differential pressure at renal artery stenoses. *Magnetic Resonance in Medicine*, 51(5), 969-977.
46. Caro, C.G.; Fitz-Gerald, J.M.; and Schroter, R.C. (1971). Atheroma and arterial wall shear observation, correlation and proposal of a shear dependent mass transfer mechanism for atherogenesis. *Proceedings of the Royal Society B: Biological Sciences*, 177(1046), 109-133.
47. Champion, J.V.; North, P.F.; Coakley, W.T.; and Williams, A.R. (1971). Shear fragility of human erythrocytes. *Biorheology*, 8(1), 23-29.
48. Drieghe, B.; Madaric, J.; Sarno, G.; Manoharan, G.; Bartunek, J.; Heyndrickx, G. R.; and DeBruyne, B. (2008). Assessment of renal artery stenosis: side-by-side comparison of angiography and duplex ultrasound with pressure gradient measurements. *European Heart Journal*, 29(4), 517-524.